Clot-Targeted Micellar Formulation Improves Anticoagulation Efficacy of Bivalirudin

Zhi-Gang She,[†,§] Xiangyou Liu,[†,§] Venkata R. Kotamraju,[†] and Erkki Ruoslahti[*,†,‡]

[†]Cancer Research Center, Sanford-Burnham Medical Research Institute, La Jolla, California 92037, United States and [‡]Center for Nanomedicine and Department of Cell, Molecular and Developmental Biology, University of California at Santa Barbara, Santa Barbara, California 93106-9610, United States. [§]These authors contributed equally to this work.

ABSTRACT Application of anticoagulants remains the primary strategy for prevention and treatment of thrombosis. However, high rate of bleeding complications limits their use. The peptide anticoagulant bivalirudin has been reported to exhibit a lower rate of bleeding complications than heparin, and it also has the advantage of not causing thrombocytopenia, which is a problem with heparin. Nonetheless, hemorrhage is the most common complication of bivalirudin therapy, and there is no effective antidote. Here we use a thrombus-binding peptide, CR(*N*Me)EKA, to accomplish selective delivery of the bivalirudin-carrying micellar nanocarrier to sites of thrombosis. Bivalirudin and CR(*N*Me)EKA, each with a PEG-lipid tail, spontaneously assembled into 30 nm micelles, which almost completely retained the anticoagulant activity of bivalirudin. The micellar formulations exhibited high stability both *in vitro* and *in vivo*. In a thromboplastin-induced mouse thrombosis model, the targeted micelles accumulated in lung thrombi 10-fold more than nontargeted micelles. Moreover, the micellar formulation significantly prolonged the half-life and thereby increased the bioavailability of bivalirudin. The micellar bivalirudin had significantly higher anticoagulant activity than free bivalirudin in both the lung thrombosis model and a ferric chloride-induced carotid artery thrombosis model. The specific targeting of thrombi demonstrated here makes it possible to increase the efficacy of bivalirudin as an anticoagulant. Alternatively, the dose could be reduced without loss of efficacy to lower the systemic exposure and improve safety.

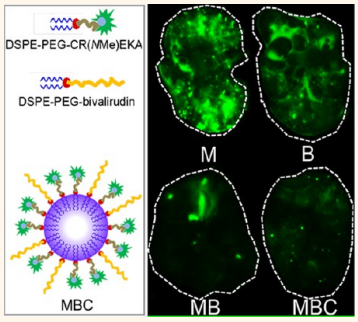

KEYWORDS: micelle · anticoagulation · bivalirudin · half-life · targeting peptide

Arterial thrombosis and venous thrombosis are common problems facing clinicians.[1] Administration of anticoagulants remains the primary strategy for prevention and treatment of thrombosis.[2] However, the rate of both ischemic events and bleeding complications still remains high during the course of such treatments.[3,4] Thrombin plays a central role in blood clotting, including pathological thrombosis.[5] It converts fibrinogen to fibrin, and it activates platelets, enhancing platelet aggregation and triggering inflammation.[6,7] These properties make thrombin an important target for anticoagulant therapies.

A variety of anticoagulants inhibit thrombin activity by directly binding to the enzyme or indirectly by activating antithrombin. Bivalirudin is a direct thrombin inhibitor that selectively and reversibly binds to the active site of free and fibrin-bound thrombin, resulting in inhibition of fibrin formation, activation of coagulant factors (V, VIII, XIII, protein C), and platelet aggregation.[8] The anticoagulant response generated by bivalirudin is more predictable than that of heparin because bivalirudin does not bind to other plasma proteins. It is not inactivated in the presence of platelet factor 4 and does not trigger thrombocytopenia like heparin does.[4,9] Bivalirudin has been reported to cause fewer bleeding complications than unfractionated heparin,[3,4,10] although there is some controversy regarding this issue according to the HEAT-PPCI study (http://www.cardiosource.org/Science-And-Quality/Clinical-Trials/H/HEAT-PPCI.aspx). Bivalirudin is approved for coronary angioplasty patients who are at high risk for bleeding.[8]

However, hemorrhage is still the most common complication of bivalirudin use,[2] and no specific antidote is available.[2,10] It is therefore desirable to develop new

* Address correspondence to ruoslahti@sanfordburnham.org.

Received for review May 30, 2014 and accepted September 29, 2014.

Published online October 01, 2014
10.1021/nn502947b

anticoagulants or improve the formulation of existing ones in order to achieve adequate anticoagulation while at the same time minimizing the bleeding risk.

Nanotechnology is showing promise in the delivery of therapeutic agents to improve therapeutic outcomes and reduce adverse effects in various diseases, including thrombosis.[11] Among various types of nanocarriers, micelles are particularly promising because of their ability to self-assemble and their small size, biocompatibility, and suitability as carriers of hydrophobic drugs.[12−14] Many micelle-based pharmaceutical formulations are currently at different stages of preclinical or clinical trials,[12] and one such agent (Genexol-PM) has been approved by the FDA for breast cancer.[14] We have previously used a clot-binding peptide (sequence: cysteine−arginine−glutamic acid−lysine−alanine or CREKA) to construct targeted micelles. The CREKA peptide was discovered by screening phage-displayed peptide libraries for tumor-homing peptides in mice and subsequently shown to target clotted plasma proteins (fibrin−fibronectin complexes) in the blood vessels and stroma of tumors.[15] CREKA also homes to the surface of atherosclerotic plaques and has been used to deliver and concentrate payloads, including bivalirudin-containing micelles, onto atherosclerotic plaques in the ApoE-null mouse model; the effect of these micelles on thrombosis, however, was not investigated.[16,17] Here, we set out to examine the delivery and efficacy of bivalirudin micelles in vascular thrombosis models using models that more closely resemble the clinical indications of bivalirudin. We also used a variant CREKA peptide that was designed to resist proteolysis and has been shown to be more effective in tumor homing than the original peptide.[18]

RESULTS AND DISCUSSION

Characteristics of the Micellar Nanocomplexes. We improved the previously published bivalirudin micelles[15] by using CR(*N*Me)EKA because we have shown that N-methylation of the glutamic acid residue protects the peptide against proteolytic degradation and improves tumor homing.[18] The general structure of the micelles containing both bivalirudin and CR(*N*Me)EKA (MBC) is depicted in Figure 1A. The controls included blank micelles (M), micelles with bivalirudin but no CR(*N*Me)EKA (MB), and CR(*N*Me)EKA-only micelles (MC).

Dynamic light scattering (DLS) measurements indicated an average hydrodynamic size of 30 nm for MBC (Figure 1B). The size distribution showed negligible changes, even after storage at 4 °C for 4 months (Figure S1 in Supporting Information), indicating high colloidal stability of the micellar nanocomplexes. Transmission electron microscopy (TEM) showed that the micelles were highly monodisperse with uniform morphology and a size of less than 50 nm, which is in accordance with the DLS results (Figure 1C). Generally, nanoparticles less than 5 nm in diameter readily leak through the kidneys into urine, while nanoparticles exceeding 150 nm are prone to being cleared by the liver and spleen.[19−21] In this regard, the size of the MBC micelles is suitable for providing slow clearance of the micelles *in vivo*.

Bivalirudin activity was almost completely retained in the micelles. The slope of each line in Figure 1D reflects the bivalirudin activity of the corresponding sample. Compared with free bivalirudin, the relative bivalirudin activities of MB and MBC were 94 and 96%, respectively.

To determine whether the MBC binds thrombin reversibly, as free bivalirudin does,[22] two-dye MBCs were constructed containing bivalirudin labeled with near-infrared dye (IRDye 800CW) and FAM-labeled CR(*N*Me)EKA. The two-dye MBC exhibited maximum absorption at 496 and 790 nm, and the corresponding emission peaks were at 520 and 800 nm (Figure S2). The FAM label was used to anchor the micelles onto magnetic beads through an anti-FAM antibody, and the other dye provided a means to monitor the stability of bivalirudin association with the micelles. The beads were incubated with thrombin, and the thrombin released from the beads after incubation at 37 °C was analyzed.[23] As shown in Figure 1E, thrombin activity was released from the thrombin-treated beads but not from untreated particles or from thrombin-treated FAM-MC. The bivalirudin label remained associated with the beads during the thrombin release (Figure S3). These results show that the micellar formulation preserves the reversibility of the bivalirudin−thrombin interaction observed in solution.

Stability of the Micellar Nanocomplexes. Stability is a significant concern in the development of micellar formulations.[24] To investigate the stability of our micelles *in vitro*, the two-dye MBCs were incubated at different pH and temperature conditions, followed by separation of intact micelles from the monomeric building blocks by centrifugation through a 10 000 Da cutoff filter. The retention rate remained more than 98% after all treatment (Figures S4A−C and S5A−C), indicating significant structural integrity of the MBC, a conclusion also supported by DLS analysis (Figures S4D and S5D).

We next studied the stability of the MBC in mouse plasma. The micelles were recovered from the plasma using anti-FAM antibody captured onto magnetic beads. The two emission peaks of the two-dye MBCs were detected in the original ratio, whereas a mixture of FAM-MBC and free IRDye 800CW PEG used as a control produced only the FAM emission peak (Figure S6). Fluorescence intensity indicated that more than 80% of the two-dye MBCs remained intact after 30 min in plasma.

The stability of MBC in the circulation *in vivo* was tested by injecting mice with two-dye MBC and by recovering the micelles from the mouse's blood 30 min later. Again, the two emission peaks were observed

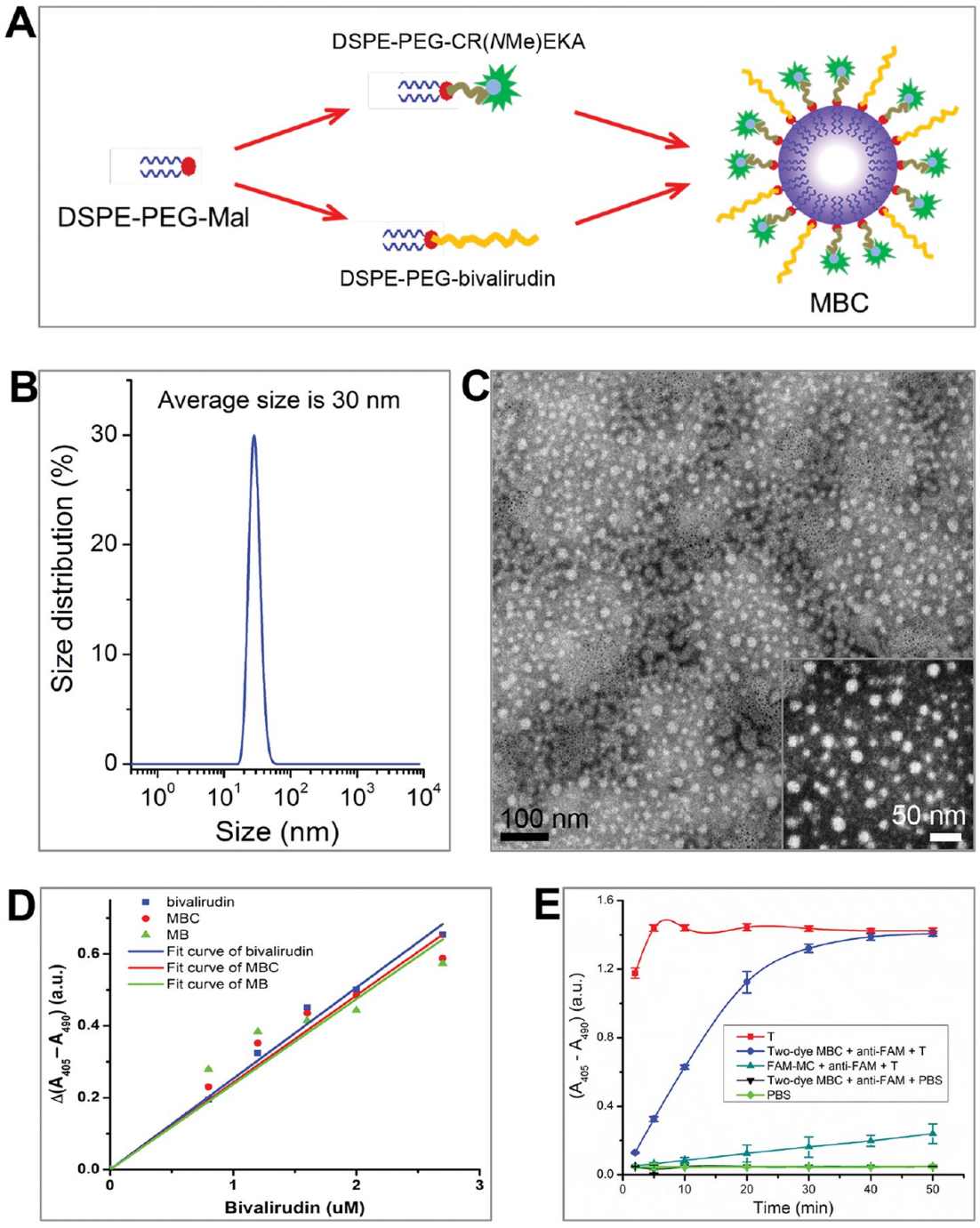

Figure 1. Preparation and characterization of micelles containing bivalirudin and CR(*N*Me)EKA (MBC). (A) Route for preparation of MBC. DSPE-PEG-Mal is 1,2-distearoyl-*sn*-glycero-3-phosphoethanolamine-*N*-[maleimide(polyethylene glycol)-2000] (ammonium salt). (B) DLS analysis of MBC. (C) TEM image of MBC after negative staining with 2% phosphotungstic acid. The inset shows the MBC particles under higher magnification. (D) Bivalirudin activity of free bivalirudin solution and bivalirudin incorporated in micelles with (MBC) or without (MB) CR(*N*Me)EKA. (E) Reversible binding of thrombin to MBC micelles. Two-dye MBC or FAM-MC (control) were anchored onto magnetic beads through an anti-FAM antibody, followed by incubation of the beads with thrombin (T) or PBS (control). Free thrombin was removed by magnetic separation, and thrombin release from the micelles was monitored by measuring thrombin activity in the supernatant.

in filter-retained fraction (Figure 2A), and the retention rate was as high as 96% (Figure 2B). The emission peak of this sample at 800 nm was significantly reduced compared with that of original micelles. This was probably caused by the different effects of plasma on the two fluorescent dyes since adding two-dye MBC into plasma reduced the intensity of emission of IRDye 800CW (Figure S7). Further, anti-FAM magnetic capture confirmed the integrity of the two-dye MBC that had circulated for 30 min (Figure 2C). Two-dye MBC injected into the circulation of mice that were subsequently subjected to lung thrombosis induction

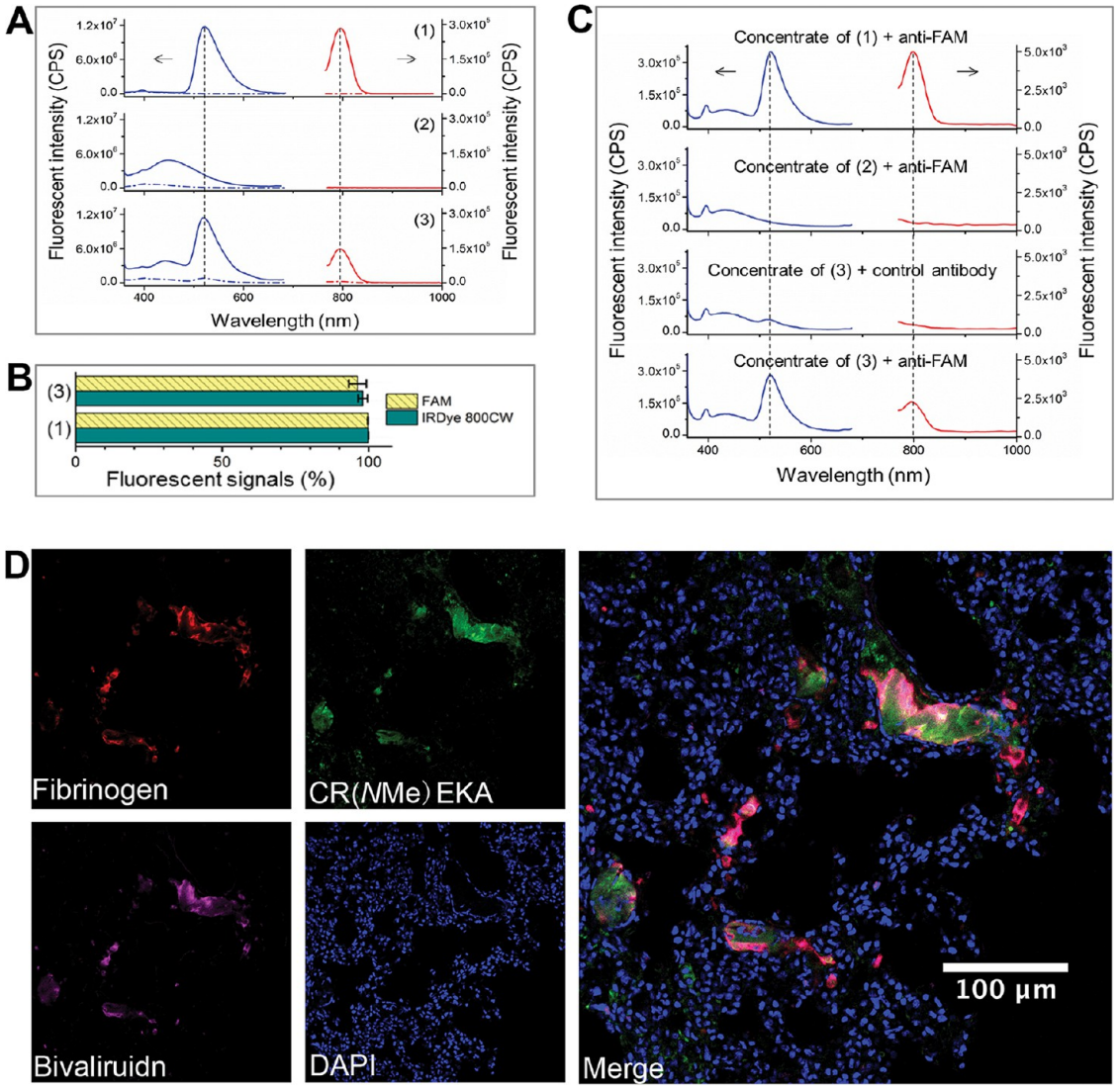

Figure 2. Stability of MBC in circulation. (A) Emission spectra of the filtrate (dashed line) and retained fraction (solid line) of two-dye MBC in PBS (1), plasma of PBS-injected mouse (2), and plasma of two-dye MBC-injected mouse (3) are shown. The micelles were allowed to circulate for 30 min. (B) Quantitative analysis of the retention rate of two-dye MBC in PBS (1) and in plasma (3) based on the results in (A). (C) Emission spectra of the retained fractions (concentrate) in (A) after anti-FAM magnetic separation. Normal IgG was used as the control antibody to show the crucial role of anti-FAM in the capture of the MBC. In (A,C), Ex = 350 nm (blue) and Ex = 760 nm (red). (D) Confocal microscopy analysis of mouse lungs 30 min after thrombosis induction following two-dye MBC injection.

showed colocalization of both the FAM and IRDye 800CW labels with fibrin(ogen) deposits (Alexa Fluor 594-labeled). This result indicates maintenance of MBC integrity in the targeted tissue (Figure 2D).

Half-Life of the Micellar Nanocomplexes. In general, a long circulation time increases the bioavailability of drugs because it gives the drug time to reach the target tissue and penetrate into it.[25] Bivalirudin has a relatively short half-life (about 25 min in humans[8]), which necessitates administration by infusion, posing a problem in some applications.[2,10] Incorporating bivalirudin into a nanocarrier of appropriate size would be expected to mitigate this problem,[26] particularly when PEG is used to reduce uptake by the reticuloendothelial system.[27,28] To determine the half-life of the micellar bivalirudin in the circulation in mice, we incorporated FAM-bivalirudin into the micelles (FAM-MB) and compared it with free FAM-bivalirudin. The blood level of intravenously injected FAM-bivalirudin exhibited a sharp decrease during the first 10 min; only about 50% was left at 10 min compared to the amount at 2 min after injection (Figure 3A). In contrast, the blood level of FAM-MB decreased only slightly within 40 min. Moreover, as estimated from the area under the curves in Figure 3A, the total amount of bivalirudin in the systemic circulation during the first 40 min after the injection was 2.3-fold higher for the micellar formulation. In another set of experiments, using longer circulating times, we measured a half-life of about 210 min for FAM-MB compared to about 20 min for

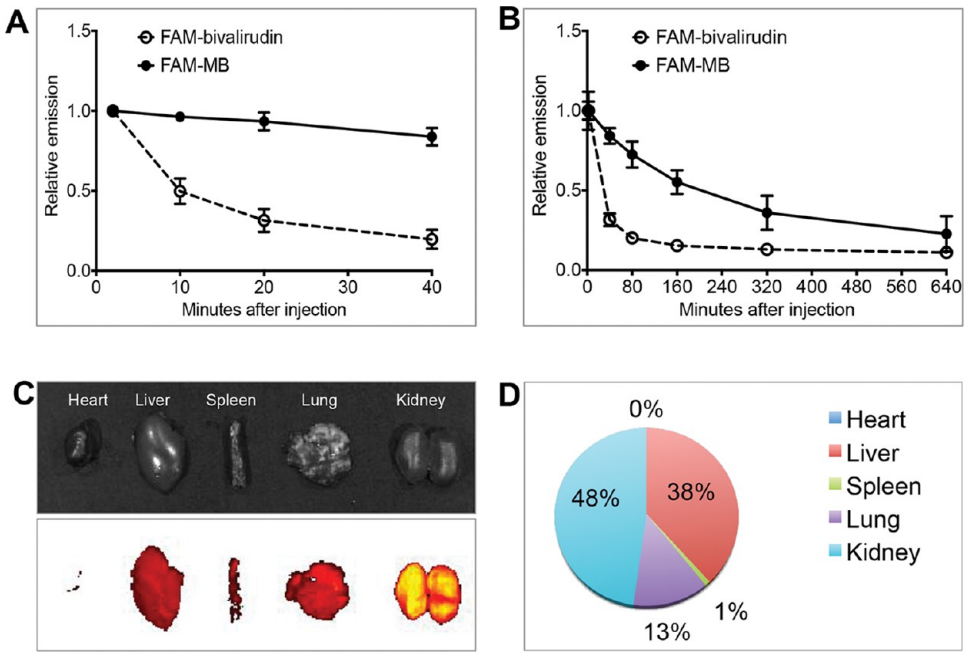

Figure 3. Half-life of free bivalirudin and bivalirudin-carrying micelles (MB). (A,B) Free FAM-bivalirudin and FAM-MB were intravenously injected into three mice in each group. The emission values at each time point were normalized to the values at 2 min after the injection. (C) Representative bright-field (top) and fluorescent (bottom) images of major mice organs collected 640 min after FAM-MB injection. (D) Quantification of the intensity of the FAM signal of major mice organs in (C).

FAM-bivalirudin (Figure 3B). Major tissues were collected and imaged for tissue distribution of the FAM-MB signal 640 min after the injection (Figure 3C). Quantification of signal indicated that FAM-MB mainly accumulated in the liver and kidneys, presumably because the micelles and their breakdown products are eliminated through these organs (Figure 3D). The prolonged blood half-life of the micellar formulation should greatly increase the bioavailability of bivalirudin.

One apparent reason for the prolonged circulation is elimination (or substantial reduction) of urinary clearance expected of a nanoparticle such as the micelles, whereas a small peptide like bivalirudin (molecular weight 2395 Da) is rapidly lost into the urine. The prolonged circulation makes it possible to maintain the required therapeutic level of bivalirudin in the blood for an extended time period and may obviate the need for continuous infusion. It may also favor accumulation of bivalirudin in thrombi.

CR(*N*Me)EKA-Promoted Homing to Thrombi *in Vivo*. To test whether CR(*N*Me)EKA increases the accumulation of the micellar nanocomplexes in the tissues containing thrombi, a mouse thrombosis model was employed.[29] In this model, intravenously injected thromboplastin triggers the clotting cascade by initiating the extrinsic pathway *via* complexation of tissue factor and factor VII, and blood clots form in tissues and embolize to the lungs.[29] The emboli can be imaged *in vivo* by preinjecting the mouse with fibrinogen tagged with a fluorophor (VivoTag-S 750) that emits in the near-infrared. To test the effect of CR(*N*Me)EKA on micelle homing, we intravenously injected mice with FAM-labeled MC (FAM-MC) or an equal dose of FAM-labeled blank micelles (FAM-M) (Figure 4A), followed 3 min later by thromboplastin to induce thrombosis. A punctate imaging signal was observed in the lungs, indicating the presence of thrombi (Figure 4B, middle panel). Quantification showed that the intensity of the lung signal was similar in the two groups (Figure 4C). Moreover, H&E staining further documented the presence of thrombi in the lungs (Figure 5). A strong VivoTag-S 750 signal was also observed in the liver and kidneys (Figure 4B,C), but relatively few thrombi were identified in the liver by H&E staining, and no thrombi were evident in the kidneys (Figure 5). The VivoTag-S 750 signal in the liver may mostly be derived from the large blood pool in this organ, which would explain the homogeneous signal (as opposed to the punctate signal from lung thrombi). The kidney signal is also likely derived from the blood, perhaps with some contribution from clearance into the urine of degradation products of the labeled fibrinogen.

FAM-MC strongly accumulated in the lungs and less so in the liver, whereas the FAM-M signal was low in both organs (Figure 4B, bottom panel). Quantification of the signal revealed a 10-fold difference in the lung and 190-fold in the liver (Figure 4D). The difference between the FAM-MC signal and the control FAM-M signal, and the fact that the FAM-MC signal accurately reflected the level of thrombosis in the tissues, shows that CR(*N*Me)EKA promotes specific homing of the micelles in thrombus-containing tissues. The specificity of CR(*N*Me)EKA micelles for lung thrombosis was confirmed by using a competition assay. The homing of FAM-CREKA to lung thrombi (Figure 4E) was

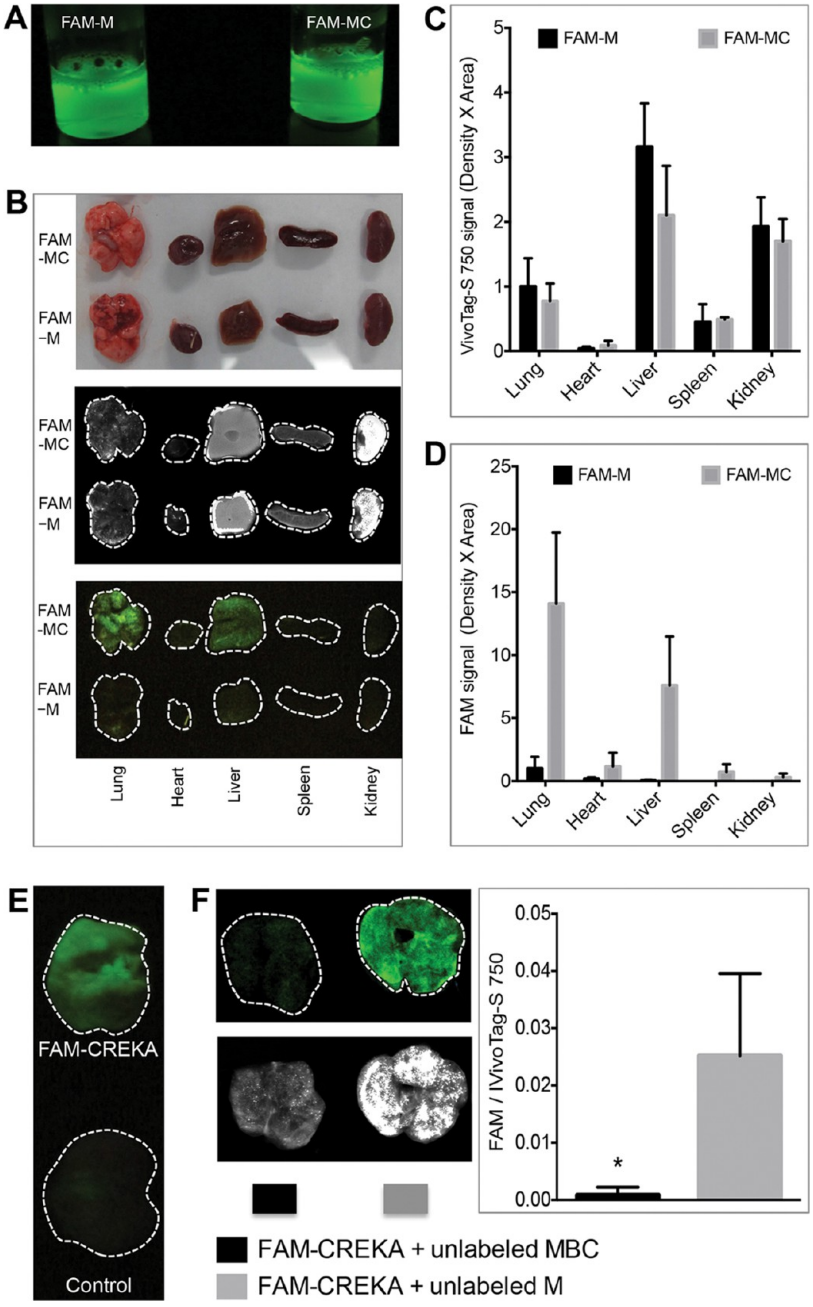

Figure 4. CR(*N*Me)EKA-guided thrombus targeting of micelles. (A) Fluorescent image of FAM-M and FAM-MC solutions under 470 nm excitation. The two solutions had the same DSPE-PEG (3.5 mM) and FAM (1.4 mM) concentration. (B) Representative images of the organs obtained with general camera in bright-field (top), Li-COR Odyssey infrared imaging system (middle), and Illumatool bright light system (bottom). (C,D) Quantification of VivoTag-S 750 (C) and FAM (D) signals in the organs of FAM-M and FAM-MC groups. *N* = 3 in each group. (E) Homing of FAM-CREKA to lung thrombosis. (F) Competitive inhibition of FAM-CREKA homing to lung thrombosis by unlabeled MBC micelles but not an unlabeled micelle vehicle. Representative images are shown in the left panel. In the right panel, CREKA homing (indicated by intensity of FAM) was quantified and normalized by the amount of thrombi (indicated by intensity of VivoTag-S 750). *N* = 3 per group.

significantly inhibited when FAM-CREKA was given mixed with unlabeled MBC at a 1:1 CREKA peptide ratio, whereas the micelle vehicle did not inhibit the homing (Figure 4F). This result shows that the CREKA peptide in the MBC is active in thrombus homing. The complete inhibition of the FAM-CREKA homing at the 1:1 mixture is likely a result of multivalent presentation of the peptide, which increases the avidity of the binding.[25] For the same reason, it was not possible to inhibit MBC homing with the CREKA peptide. This CREKA effect can be used to increase the delivery of bivalirudin to the sites of thrombosis and reduce the systemic exposure to the drug.

Anticoagulant Efficacy of Micellar Bivalirudin in the Lung Thrombosis Model. To investigate whether targeted micellar formulation would enhance the efficacy of bivalirudin in inhibiting lung thrombus formation,

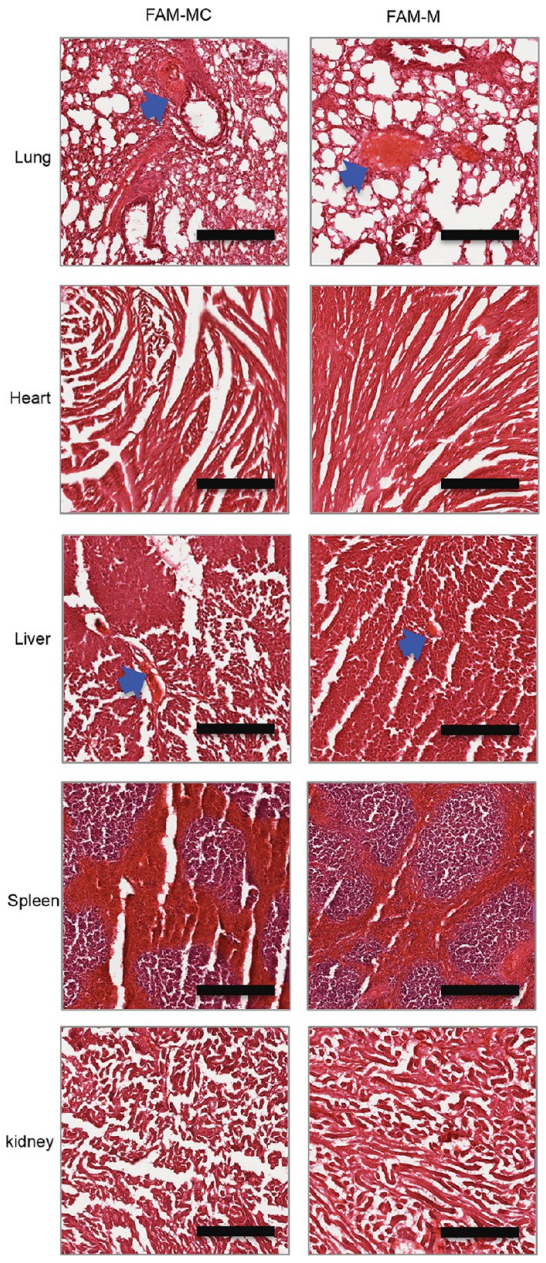

Figure 5. H&E staining of organs from FAM-MC- or FAM-M-injected mice with thromboplastin-induced lung thrombosis. *N* = 3 in each group. The arrows indicate the thrombi formed. Scale bars are 100 μm.

three different doses of the bivalirudin formulations were tested in the lung thrombosis model. The thrombosis was initiated 3 min after the bivalirudin injection (Figure 6A). At the dose of 0.5 μmol/kg body weight, none of the reagents was effective (Figure 6C). At 1 μmol/kg body weight, the micellar formulations of bivalirudin were active (Figure 6B,C). MBC strongly inhibited thrombosis; the nontargeted bivalirudin micelles (MB) seemed slightly active, and free bivalirudin was no more active than the negative control, blank micelles (M). MBCs were at least 4 times more effective at this dose than free bivalirudin. At the 2 μmol/kg dose, MB and free bivalirudin showed significant

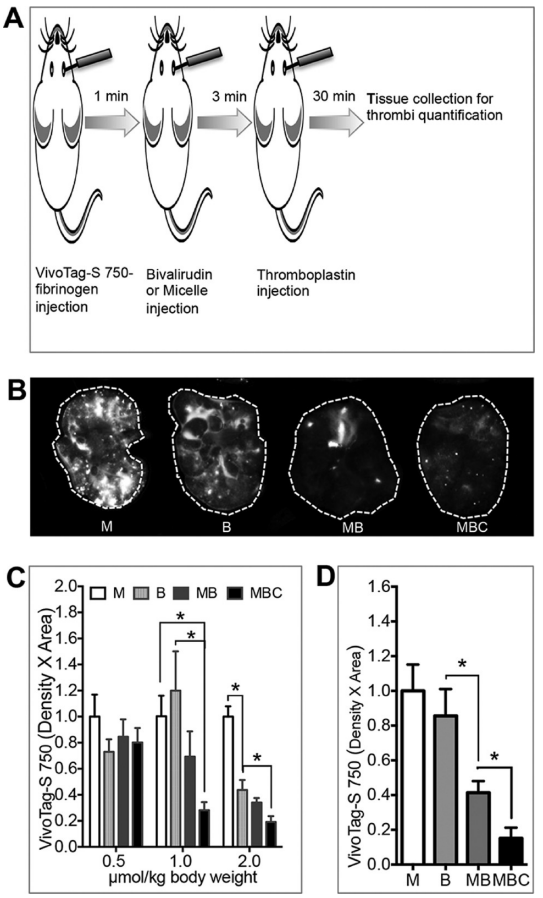

Figure 6. Micellar formulation improves the anticoagulant efficacy of bivalirudin in thromboplastin-induced lung thrombosis model. (A) Schematic of the model construction and treatment procedures. (B) Representative images of lung thrombosis indicated by the fluorescent VivoTag-S 750 signal in the 1 μmol/kg group. (C) Quantification of VivoTag-S 750 signal in the lungs. *N* = 14–15. (D) Effect of MBC on lung thrombosis was also evaluated by injecting 1 μmol/kg body weight of MBC 10 min (rather than 3 min) prior to induction of lung thrombosis by thromboplastin injection.

inhibition of thrombosis, but the MBCs were again the most effective formulation (Figure 6C). The lung thrombosis-inhibiting effect of MBC was even better than a 2-fold dose of free bivalirudin (Figure 6C), underscoring the potential of targeted the micellar formulation in lowering the dose of bivalirudin required for thrombosis inhibition. The effect of the bivalirudin formulations on lung thrombosis was also evaluated by injecting 1 μmol/kg body weight of MBC 10 min prior to lung thrombosis induction. In this time frame, free bivalirudin was again no more effective than blank micelles (M), whereas MB was active but less so than MBC (Figure 6D). The difference between the activities of MB and free bivalirudin likely reflects the longer half-life of the micellar formulation. Finally, toxicity studies showed that MBC and free bivalirudin shared the same light liver toxicity (Figure S8).

Anticoagulant Efficacy of Micellar Bivalirudin in $FeCl_3$-Induced Carotid Artery Thrombosis Model. We next sought to determine whether the targeted bivalirudin micelles would

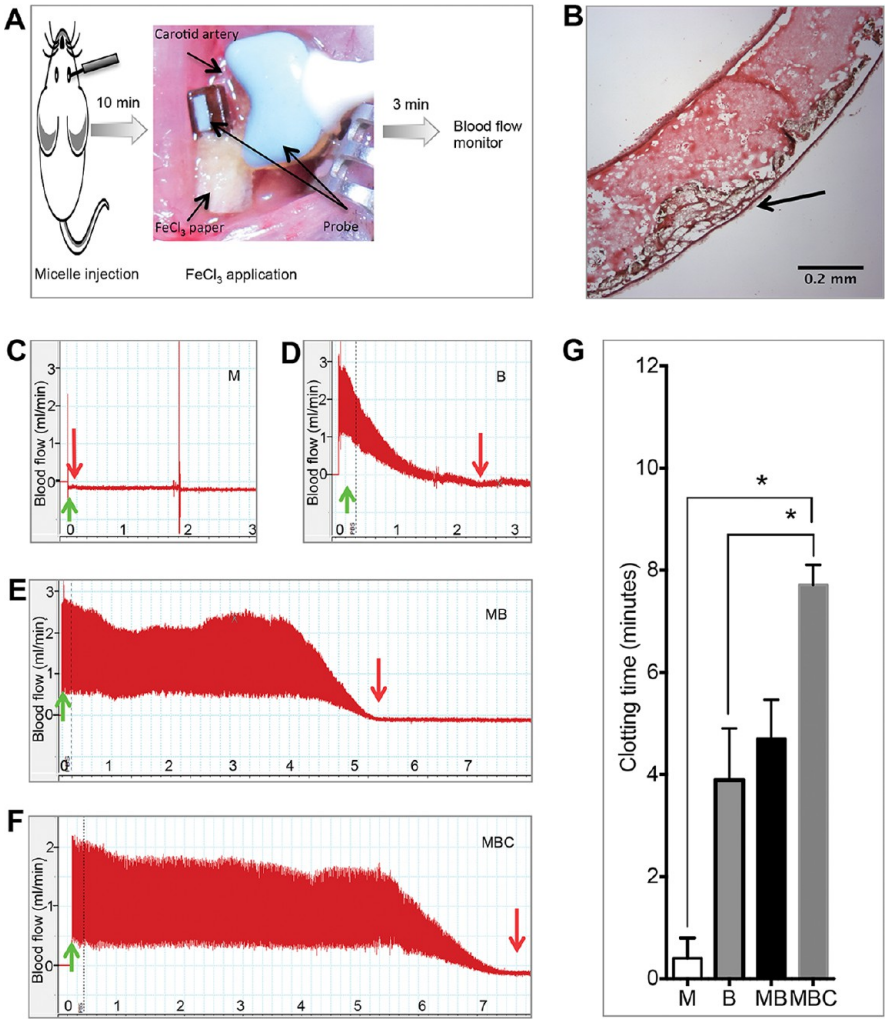

Figure 7. Micellar formulation improves the anticoagulant efficacy of bivalirudin in $FeCl_3$-induced carotid artery thrombosis model. (A) Schematic of the model construction and the procedure. (B) Representative image of $FeCl_3$-induced thrombi formed in the carotid artery. The arrow indicates the site where the filter paper saturated with 40% $FeCl_3$ was placed. (C–F) Representative images of blood flow changes in M (C), B (D), MB (E), and MBC (F) groups. Green arrows indicate the beginning of blood flow monitoring. Red arrows indicate the time when blood flow had completely stopped. The numbers on the *x*-axis are minutes of monitoring. (G) Clotting times in different groups. *N* = 4, 13, 8, and 12 in M, B, MB, and MBC groups, respectively.

also show superior activity in arterial thrombosis. For this purpose, an $FeCl_3$-induced mouse carotid artery thrombosis model was constructed and tested (Figure 7A).[30] Different from the lung thrombosis model, the thrombosis in this model is in the systemic circulation. Also, the clotting cascade is triggered differently, by docking of ferric ions onto endothelial-associated red blood cells. The resulting clot is also different in that it is rich in red cells.[31] In our hands, an optimal level of thrombosis for the measurement of anticoagulant activity was obtained by treating the exposed carotid artery with a 40% $FeCl_3$ solution for 3 min (Figure 7A). Figure 7B shows the microscopic appearance of the resulting thrombi in the carotid artery.

In the $FeCl_3$ procedure, complete clotting occurred in the vehicle control (blank micelles) group about 24 s after the removal of the $FeCl_3$-saturated filter paper (Figure 7C,G). Injection of free bivalirudin at the dose of 1 μmol/kg postponed the clotting time (Figure 7D,G) to 3.9 min. MB with the same amount of bivalirudin seemed to be more effective (clotting time 4.7 min) than free bivalirudin, but the difference was not significant (Figure 7E,G). In contrast, injection of MBC with the same amount of bivalirudin as in the free bivalirudin injection significantly prolonged the clotting time to 7.7 min (Figure 7F,G). Thus, MBC exhibited significantly higher efficacy in inhibiting $FeCl_3$-induced carotid artery thrombosis than the same dose of free bivalirudin.

The likely primary reason for the enhanced efficacy of MBC and MB is the prolonged circulation time demonstrated above. Multivalent interactions can improve the binding affinity of multiple ligands on one molecular entity to receptors.[25,32] Thus, another factor enhancing the activity of both the micellar formulations may be the multivalent display of bivalirudin in the micelle, which may increase the avidity of bivalirudin to thrombin. Most importantly, the difference between MBC and MB reflects the contribution of the

CR(*N*Me)EKA targeting. As shown above, it greatly increases the accumulation of the micelles in the thrombus area, creating a high local concentration of bivalirudin. Time course studies would be needed to fully elucidate the contributions of the micellar formulation and targeting to the superior activity of the targeted micelles. The long half-life of the MBC micelles may allow expansion of the indications of bivalirudin use. There is no specific treatment for most thrombophilias, and recurrent thrombosis may require long-term preventative anticoagulation.[33] As an injectable, the MBC formulation will not be suitable for long-term anticoagulation therapy, but expansion of the indications to subacute thrombosis may be possible.

CONCLUSION

Anticoagulant therapies must balance the reduction of thrombotic complications with the risk of periprocedural bleeding.[4] In this paper, we describe a strategy to improve the anticoagulant activity, targeted delivery of a micellar bivalirudin formulation to thrombus-enriched tissues. We show that bivalirudin can be formulated into the micellar structure with near complete retention of activity and high stability, and that the micellar form greatly increases the half-life of the drug in the circulation. Targeting of the micelles with a clot-homing peptide further increased the anticoagulant efficacy in two distinct thrombosis models. The bivalirudin micelles may merit clinical translation, but it should also be noted that what we have developed is a general platform technology that can be applied to other anticoagulants with side effects, such as heparin. Finally, the hydrophobic center of the micelle could be exploited in the delivery of a second drug to areas of clotting.

MATERIALS AND METHODS

Animal Use. C57BL/6J mice were purchased from the Jackson Laboratory. All procedures on the animals, including minimizing discomfort, were carried out according to the protocol approved at the Sanford-Burnham Medical Research Institute.

Materials. 1,2-Distearoyl-*sn*-glycero-3-phosphoethanolamine-*N*-[maleimide(polyethylene glycol)-2000] (ammonium salt) (DSPE-PEG-Mal) was purchased from Avanti Polar Lipids, *N*-acetyl-L-cysteine methyl ester from Sigma-Aldrich, IRDye 800CW NHS ester from Li-COR, and VivoTag-S 750 from PerkinElmer. Fibrinogen and thromboplastin were from Sigma-Aldrich. The peptides, bivalirudin, FAM-bivalirudin, CR(*N*Me)EKA, and FAM-CR(*N*Me)EKA, were all synthesized in our laboratory as described.[16] A cysteine residue was added to the N-terminus of bivalirudin for conjugation purposes.

Preparation and Characterization of Micelles. The micellar nanocomplexes were prepared according to the procedures described previously,[16] with some modifications. Briefly, cysteine-containing peptides (bivalirudin, FAM-bivalirudin, CR(*N*Me)EKA, and FAM- CR(*N*Me)EKA) or FAM-cysteine were conjugated to DSPE-PEG-Mal *via* thioether linkage. To prepare MBC micelles, DSPE-PEG-bivalirudin and DSPE-PEG-CR(*N*Me)EKA were mixed in a molar ratio of 2:3 in methanol. The mixture was evaporated under nitrogen flow to form a dry film. The film was further dried under vacuum overnight and then rehydrated with 50 °C prewarmed degassed water, followed by sonication to produce a clear micelle solution. The resulting micelle samples were dialyzed against PBS using Slide-A-Lyzer 3.5K dialysis cassettes (Thermo) for 24 h at 4 °C. After dialysis, the micelle solution was filtered through a 0.22 μm filter. The other micelles were prepared following the similar procedure (for more details, see Table S1 in Supporting Information).

All of the micellar formulations were kept at 4 °C until use. DLS (Malvern Zetasizer Nano ZS90) was used to determine the hydrodynamic size of the micelles. TEM observation was performed on a JEOL JEM-1200EX II electron microscope operating at 80 kV.

Measurement of Bivalirudin Activity. *In vitro* bivalirudin activity was measured using a commercial chromogenic assay kit purchased from diaPharma according to the manufacturer's instructions. Serial dilutions of bivalirudin samples, and PBS as control, were incubated in a 96-well plate with an excess of thrombin at 37 °C for 2 min, followed by addition of the chromogenic substrate S-2366 (diaPharma) and incubation at 37 °C for another 2 min. Then, 20% (v/v) acetic acid was added, and the difference of absorbance at 405 and 490 nm (reference wavelength) in each well, denoted as A405−A490, was measured. The difference in (A405−A490) between the PBS wells and the bivalirudin wells, denoted as Δ(A405−A490), was proportional to the amount of active bivalirudin in the samples. A linear regression of Δ(A405−A490) plotted against bivalirudin concentration was prepared. The slope of the line reflects the bivalirudin activity in the samples, with a steeper slope indicating higher bivalirudin activity. At the same bivalirudin concentration, higher bivalirudin activity resulted in higher Δ(A405−A490) value.

Reversible Binding of Thrombin to MBC. FAM-MC and two-dye MBC (both in 250 μL and 180 μM of CR(*N*Me)EKA) were incubated with 5 μL of antifluorescein/Oregon Green antibody (Life Technologies, A889) at 4 °C overnight. Protein A/G magnetic beads (50 μL, 10 mg/mL, Pierce) were then added into each sample, followed by mixing at room temperature for 8 h, magnetic separation, and five PBS washes. Thrombin (100 μL, 10 mg/mL, diaPharma) or PBS (100 μL) was then added into the test tube, followed by incubation at 37 °C for 3 min, magnetic separation, and three PBS washes. After being washed, the magnetic beads were resuspended in PBS (100 μL) and incubated at 37 °C for 30 min. The beads were then magnetically separated, and the supernatant (90 μL/well) was collected and transferred into a 96-well plate. Free thrombin (90 μL/well, 10 mg/mL) and PBS blank (90 μL/well) were also used as controls. The S-2366 substrate (30 μL/well) was added, and A405−A490 was measured at different time points.

Stability of micellar complexes. *In Vitro Stability.* Two-dye MBCs (10 μM) in PBS (pH7.4, 500 μL) were incubated at different temperatures (4, 23, and 37 °C) or at 37 °C in different buffers (pH 5.1, 6.4, 7.4, and 8.8) for different periods of time (0.5, 1, 6, 12, and 24 h). After the treatment, the samples were centrifuged (2000*g*, 10 min, 4 °C) in Amicon Ultra-0.5 centrifugal filter devices (MWCO = 10K). The filtrate and the retained fraction (concentrate) were examined in a HORIBA fluoroMax-4 spectrofluorometer at excitation (Ex) of 350 and 760 nm. The retention rate of micelle sample was calculated as follows:

Retention rate based on FAM signal (%) = 100 × $Em_{c520\ nm}/(Em_{c520\ nm} + Em_{f520\ nm})$; retention rate based on IRDye 800CW signal (%) = 100 × $Em_{c800\ nm}/(Em_{c800\ nm} + Em_{f800\ nm})$. $Em_{c520\ nm}$, $Em_{f520\ nm}$, $Em_{c800\ nm}$, and $Em_{f800\ nm}$ are the emission peak intensities of the concentrate and filtrate at 520 nm (Ex = 350 nm) and 800 nm (Ex = 760 nm).

DLS measurements were carried out as follows: MBC without any dye labeling was subjected to the same treatments as above, and the samples were analyzed using a Malvern Zetasizer Nano ZS90.

Stability in Plasma. Normal mouse plasma was mixed with a micelle sample, followed by incubation at 37 °C for 30 min. The incubated samples, two-dye MBC (250 μL, 36 μM), two-dye MBC (250 μL, 36 μM) in plasma, plasma (250 μL), and a mixture of FAM-MBC (150 μL, 60 μM) and IRDye 800CW PEG (100 μL; LI-COR) were mixed with anti-FAM (5 μL, 1 mg/mL) or 10 μL normal rabbit control IgG (0.5 mg/mL, Santa Cruz) and then incubated at 4 °C overnight. Protein A/G magnetic beads (50 μL, 10 mg/mL, Pierce) were subsequently added into each sample, followed by mixing at room temperature for 8 h. After washing and eluting according to the manufacturer's instructions, the supernatant was collected, its pH was adjusted to neutral, and the emission spectra were measured at Ex of 350 and 760 nm.

In Vivo Stability. Two-dye MBCs in PBS (pH 7.4) (200 μL, 180 μM) or PBS (200 μL) were intravenously injected into mice. Plasma was collected 30 min after the injection and fractionated in Amicon Ultra-0.5 centrifugal filter devices (MWCO = 10K; 2000*g*, 10 min, 4 °C), and the emission spectra of the filtrate and retained fraction were measured under Ex 350 and 760 nm. The retention rate was calculated as detailed above. The retained fraction (125 μL) was diluted with PBS to 500 μL, followed by magnetic separation as described above. The original two-dye MBC (500 μL, 72 μM) was a positive control. The eluate from the beads was adjusted to neutral pH. The emission spectra were measured at Ex 350 and 760 nm.

Confocal Microscopy. Collected lung tissues were fixed with 4% PFA for 2 h, dehydrated in 20% sucrose overnight, frozen in OCT, and sliced into 10 μm sections. The sections were penetrated with 0.1% Triton-X 100 PBS for 10 min and mounted with DAPI containing mounting medium. A BioRad inverted Radiance 2100 multiphoton confocal microscope was used to obtain images, followed by ImageJ software.

Half-Life Measurement. FAM-bivalirudin and FAM-MB were intravenously injected into C57 BL/6J mice. Blood samples were collected into heparinized vacutainers 2, 10, 20, and 40 min after the injection. In another set of experiments, blood samples were collected into heparinized vacutainers 2, 40, 80, 160, 320, and 640 min after the injection. After centrifugation at 300*g* for 10 min, the supernatant was collected, diluted 10 times with PBS, and the fluorescent intensity of FAM was measured using a microplate reader. Major tissues were collected for IVIS200 imaging.

Lung Thrombosis Model. Mouse lung thrombosis model was constructed as described[29] with modification. The mice were intravenously injected with VivoTag-S 750 or Alexa Fluor 594-labeled fibrinogen (2 nmol/30 g body weight) and 1 min later, with the test compounds, followed by induction of thrombosis with thromboplastin (4 μL/g body weight) 3 or 10 min later. The mice were sacrificed 30 min later. The lungs and other organs were collected, washed with PBS, and imaged using Li-COR Odyssey infrared imaging system. The lungs of blank control mice, which were injected only with thromboplastin, were used to calibrate the fluorescence excitation. The VivoTag-S 750 signal intensity was quantified using Image Pro Plus software (Media Cybernetics, Inc., Warrendale) to reflect the amount of thrombi formed in the lungs.

Targeting of Micelles to Clotting Sites. The lung thrombosis model was used to study the targeting of micelles. The procedure described above was used with minor modifications: 1 min after VivoTag-S 750-labeled fibrinogen was injected, the mice were injected with same amount (7 μM FAM/kg body weight) of FAM-M or FAM-MC. The mice were sacrificed 30 min after the thromboplastin injection, and the major organs were collected, washed with PBS, and imaged with a general camera in bright field and with a Li-COR Odyssey infrared imaging system and Illumatool bright light system. The collected organs were sectioned, H&E stained, and scanned with a ScanScope XT system to monitor thrombosis.

To study competitive inhibition of homing to lung thrombi, FAM-CREKA (3 μM FAM/kg body weight), FAM-CREKA and MBC mixture at a ratio of 1:1 (based on the CREKA peptide), or FAM-CREKA mixture with M (with the same amount micelles as in the FAM-CREKA-MBC mixture) was injected after the fluorescent fibrinogen injection, and the lungs were imaged as above.

Carotid Artery Thrombosis Model. Mouse carotid artery thrombosis model was constructed as described[30] with modifications. Mice were anesthetized with intraperitoneal injection of Avertin. Subsequently, they were intravenously injected with M, free bivalirudin (B, 1 μmol/kg), MB, or MBC. The doses for MB and MBC were calibrated to the same active bivalirudin amount as in B. The left carotid artery was then exposed and freed from the surrounding tissue under a dissecting microscope. An ultrasonic flow probe (0.5VB, Transonic Systems) was placed around the artery. Ten minutes after the injection of the test compounds, a piece (1 × 2 mm) of filter paper saturated with 40% $FeCl_3$ was placed on the exposed carotid artery. Three minutes later, the filter paper was removed, the wound was filled with PBS, and blood flow monitoring was initiated to record the clotting time until blood flow completely stopped (the blood flow curve came down to 0).

Blood Chemistry Panel. Blood was collected from the orbital plexus into lithium heparin collection tubes and centrifuged at 300*g*, and plasma was collected. Plasma (100 μL) was pipetted into a Comprehensive Diagnostic profile rotor #500-1038 and analyzed using the VetScan VS2. The results were evaluated by prism using two-way ANOVA. $N = 5$ in each group.

Statistical Analyses. All values presented represent mean ± SEM. Statistical differences between two data sets were determined using the Students *t* test. A value of $P < 0.05$ was considered statistically significant. ANOVA followed by Tukey's multiple comparisons test was used to compare more than two sets of data.

Conflict of Interest: The authors declare the following competing financial interest(s): E.R. is a shareholder and consultant of EnduRx Pharmaceuticals Inc. and has ownership interest (including patents) in the same. No potential conflicts of interest were disclosed by the other authors.

Acknowledgment. This work was supported by a grant from EnduRx Inc.

Supporting Information Available: Supplementary Table S1 and Figures S1−S8. This material is available free of charge *via* the Internet at http://pubs.acs.org.

REFERENCES AND NOTES

1. Anderson, J. A.; Weitz, J. I. Hypercoagulable States. *Crit. Care Clin.* **2011**, *27*, 933–952.
2. Alquwaizani, M.; Buckley, L.; Adams, C.; Fanikos, J. Anticoagulants: A Review of the Pharmacology, Dosing, and Complications. *Curr. Emerg. Hosp. Med. Rep.* **2013**, *1*, 83–97.
3. Hartmann, F. Safety and Efficacy of Bivalirudin in Acute Coronary Syndromes. *Curr. Pharm. Des.* **2008**, *14*, 1191–1196.
4. Rao, S. V.; Ohman, E. M. Anticoagulant Therapy for Percutaneous Coronary Intervention. *Circ.: Cardiovasc. Interventions* **2010**, *3*, 80–88.
5. Davie, E. W.; Kulman, J. D. An Overview of the Structure and Function of Thrombin. *Semin. Thromb. Hemostasis* **2006**, *32* (Suppl 1), 3–15.
6. Coughlin, S. R. Thrombin Signalling and Protease-Activated Receptors. *Nature* **2000**, *407*, 258–264.
7. Chesebro, J. H.; Zoldhelyi, P.; Badimon, L.; Fuster, V. Role of Thrombin in Arterial Thrombosis: Implications for Therapy. *Thromb. Haemostasis* **1991**, *66*, 1–5.
8. Di Nisio, M.; Middeldorp, S.; Buller, H. R. Direct Thrombin Inhibitors. *N. Engl. J. Med.* **2005**, *353*, 1028–1040.
9. Weitz, J. I.; Crowther, M. Direct Thrombin Inhibitors. *Thromb. Res.* **2002**, *106*, V275–284.
10. Warkentin, T. E.; Greinacher, A.; Koster, A. Bivalirudin. *Thromb. Haemostasis* **2008**, *99*, 830–839.
11. Ilinskaya, A. N.; Dobrovolskaia, M. A. Nanoparticles and the Blood Coagulation System. Part I: Benefits of Nanotechnology. *Nanomedicine* **2013**, *8*, 773–784.
12. Torchilin, V. P. Micellar Nanocarriers: Pharmaceutical Perspectives. *Pharm. Res.* **2007**, *24*, 1–16.
13. Peer, D.; Karp, J. M.; Hong, S.; Farokhzad, O. C.; Margalit, R.; Langer, R. Nanocarriers as an Emerging Platform for Cancer Therapy. *Nat. Nanotechnol.* **2007**, *2*, 751–760.

14. Oerlemans, C.; Bult, W.; Bos, M.; Storm, G.; Nijsen, J. F.; Hennink, W. E. Polymeric Micelles in Anticancer Therapy: Targeting, Imaging and Triggered Release. *Pharm. Res.* **2010**, *27*, 2569–2589.
15. Simberg, D.; Duza, T.; Park, J. H.; Essler, M.; Pilch, J.; Zhang, L.; Derfus, A. M.; Yang, M.; Hoffman, R. M.; Bhatia, S.; *et al.* Biomimetic Amplification of Nanoparticle Homing to Tumors. *Proc. Natl. Acad. Sci. U.S.A.* **2007**, *104*, 932–936.
16. Peters, D.; Kastantin, M.; Kotamraju, V. R.; Karmali, P. P.; Gujraty, K.; Tirrell, M.; Ruoslahti, E. Targeting Atherosclerosis by Using Modular, Multifunctional Micelles. *Proc. Natl. Acad. Sci. U.S.A.* **2009**, *106*, 9815–9819.
17. Hamzah, J.; Kotamraju, V. R.; Seo, J. W.; Agemy, L.; Fogal, V.; Mahakian, L. M.; Peters, D.; Roth, L.; Gagnon, M. K.; Ferrara, K. W.; *et al.* Specific Penetration and Accumulation of a Homing Peptide within Atherosclerotic Plaques of Apolipoprotein E-Deficient Mice. *Proc. Natl. Acad. Sci. U.S.A.* **2011**, *108*, 7154–7159.
18. Agemy, L.; Sugahara, K. N.; Kotamraju, V. R.; Gujraty, K.; Girard, O. M.; Kono, Y.; Mattrey, R. F.; Park, J. H.; Sailor, M. J.; Jimenez, A. I.; *et al.* Nanoparticle-Induced Vascular Blockade in Human Prostate Cancer. *Blood* **2010**, *116*, 2847–2856.
19. Mitragotri, S.; Lahann, J. Physical Approaches to Biomaterial Design. *Nat. Mater.* **2009**, *8*, 15–23.
20. Duan, X.; Li, Y. Physicochemical Characteristics of Nanoparticles Affect Circulation, Biodistribution, Cellular Internalization, and Trafficking. *Small* **2013**, *9*, 1521–1532.
21. Wang, Q.; Zhuang, X.; Mu, J.; Deng, Z. B.; Jiang, H.; Zhang, L.; Xiang, X.; Wang, B.; Yan, J.; Miller, D.; *et al.* Delivery of Therapeutic Agents by Nanoparticles Made of Grapefruit-Derived Lipids. *Nat. Commun.* **2013**, *4*, 1867.
22. Shammas, N. W. Bivalirudin: Pharmacology and Clinical Applications. *Cardiovasc. Drug Rev.* **2005**, *23*, 345–360.
23. Parry, M. A.; Maraganore, J. M.; Stone, S. R. Kinetic Mechanism for the Interaction of Hirulog with Thrombin. *Biochemistry* **1994**, *33*, 14807–14814.
24. Kim, S.; Shi, Y.; Kim, J. Y.; Park, K.; Cheng, J. X. Overcoming the Barriers in Micellar Drug Delivery: Loading Efficiency, *In Vivo* Stability, and Micelle–Cell Interaction. *Expert Opin. Drug Delivery* **2010**, *7*, 49–62.
25. Ruoslahti, E.; Bhatia, S. N.; Sailor, M. J. Targeting of Drugs and Nanoparticles to Tumors. *J. Cell Biol.* **2010**, *188*, 759–768.
26. Moghimi, S. M.; Hunter, A. C.; Murray, J. C. Long-Circulating and Target-Specific Nanoparticles: Theory to Practice. *Pharmacol. Rev.* **2001**, *53*, 283–318.
27. Schipper, M. L.; Iyer, G.; Koh, A. L.; Cheng, Z.; Ebenstein, Y.; Aharoni, A.; Keren, S.; Bentolila, L. A.; Li, J.; Rao, J.; *et al.* Particle Size, Surface Coating, and PEGylation Influence the Biodistribution of Quantum Dots in Living Mice. *Small* **2009**, *5*, 126–134.
28. Wen, S.; Zhao, Q.; An, X.; Zhu, J.; Hou, W.; Li, K.; Huang, Y.; Shen, M.; Zhu, W.; Shi, X. Multifunctional Pegylated Multi-walled Carbon Nanotubes for Enhanced Blood Pool and Tumor MR Imaging. *Adv. Healthcare Mater.* **2014**, 10.1002/adhm.201300631.
29. Lin, K. Y.; Kwong, G. A.; Warren, A. D.; Wood, D. K.; Bhatia, S. N. Nanoparticles That Sense Thrombin Activity as Synthetic Urinary Biomarkers of Thrombosis. *ACS Nano* **2013**, *7*, 9001–9009.
30. Day, S. M.; Reeve, J. L.; Myers, D. D.; Fay, W. P. Murine Thrombosis Models. *Thromb. Haemostasis* **2004**, *92*, 486–494.
31. Barr, J. D.; Chauhan, A. K.; Schaeffer, G. V.; Hansen, J. K.; Motto, D. G. Red Blood Cells Mediate the Onset of Thrombosis in the Ferric Chloride Murine Model. *Blood* **2013**, *121*, 3733–3741.
32. Englund, E. A.; Wang, D.; Fujigaki, H.; Sakai, H.; Micklitsch, C. M.; Ghirlando, R.; Martin-Manso, G.; Pendrak, M. L.; Roberts, D. D.; Durell, S. R.; *et al.* Programmable Multivalent Display of Receptor Ligands Using Peptide Nucleic Acid Nanoscaffolds. *Nat. Commun.* **2012**, *3*, 614.
33. Kyrle, P. A.; Rosendaal, F. R.; Eichinger, S. Risk Assessment for Recurrent Venous Thrombosis. *Lancet* **2010**, *376*, 2032–2039.